



State-of-health estimator based-on extension theory with a learning mechanism for lead-acid batteries

Kuei-Hsiang Chao*, Jing-Wei Chen

Department of Electrical Engineering, National Chin-Yi University of Technology, Taiwan

ARTICLE INFO

Keywords:

Lead-acid batteries
Extension matter-element model
State-of-health (SOH) estimator
Coup de fouet voltage
Programmable system-on-chip
microcontroller

ABSTRACT

The main objective of this paper is to design and implement an improved intelligent state-of-health (SOH) estimator for estimating the useful life of lead-acid batteries. Laboratory studies were carried out to measure and record the distributed range of characteristic values in each SOH cycle for the battery subject to cycles of charging and discharging experiments. The measured coup de fouet voltage, internal resistance, and transient current are used as characteristics to develop an intelligent SOH evaluation algorithm. This method is based on the extension matter-element model that has been modified in this research by adding a learning mechanism for evaluation SOH of batteries. The proposed algorithm is relatively simple so that it can be easily implemented with a programmable system-on-chip (PSOC) microcontroller achieve rapid evaluation of battery SOH with precision by using a concise hardware circuit.

© 2011 Elsevier Ltd. All rights reserved.

1. Introduction

For most normal lead-acid batteries, state-of-health (SOH) is determined by measuring the usable capacity of a fully-charged lead-acid battery. In past literature, besides direct use of the Coulometric measurement method, there are lead-acid battery SOH estimation approaches (Robinson, 1996), as characterized in terminal voltage, internal resistance, operating temperature, and the voltage phase angle, which is measured after AC current input to batteries. However, these characteristic values generally vary with battery aging, thus exacerbating SOH estimation. Recently, many expert scholars suggest analysis of the coup de fouet voltage derived at the initial discharge period of a fully-charged lead-acid battery, and thus the SOH of a lead-acid battery could be estimated from its trough value, plateau voltage, or occurring time (Bose & Laman, 2000). Compared with other characteristics, the tendency of coup de fouet plateau voltage versus battery usable capacity is the most linear, thus, using this characteristic to estimate SOH of battery life can achieve accuracy to some extent. There have been many studies on the coup de fouet voltage of a lead-acid battery (Anbuky & Pascoe, 2000; Pascoe & Anbuky, 2005), such as Prof. Pascoe et al., which reported that lead-acid battery coup de fouet voltage can definitely reveal the current SOH of a battery. However, experts failed to determine a definite interpretation of such phenomenon until 2006, when Prof. Delaille et al. (Delaille, Perrin, Huet, & Hernout, 2006) reported that this was primarily a transient

phenomenon arising from redox reaction between a sulfuric acid electrolyte (H_2SO_4) in a positive electrode container and a lead sulfide ($PbSO_4$) on a positive electrode plate, in a battery unit. This phenomenon is not restricted to occur in a fully-charged lead-acid battery at the time of discharge moment. In fact, when maintaining and stabilizing a lead-acid battery electrolyte for a period of time, both charging and discharge behaviors would induce such coup de fouet phenomenon (Delaille et al., 2006). When measuring the coup de fouet voltage of a lead-acid battery, the charging/discharging state must be controlled for achieving the measurement condition with one accord. Therefore, it remains difficult to determine the battery SOH simply from the coup de fouet voltage of a lead-acid battery.

In order to improve the lead-acid battery SOH estimation accuracy, many studies have employed intelligent algorithms to estimate the lead-acid battery life state, such as the neural network (Kim et al., 2009; Valdez et al., 2006), fuzzy (Shen et al., 2002; Spath, Jossen, Doring, & Garche, 1997; Wang, Wang, Lee, & Tseng, 1995) and neuro-fuzzy (Jang, 1996; Lin & Lee, 1999; Oh, Pedrycz, & Park, 2006; Pascoe & Anbuky, 2001) algorithms, and combined multiple characteristics representing the lead-acid battery SOH to study the relationship between each characteristics and data of each battery SOH, thereby improving recognition accuracy. Nonetheless, data distribution of lead-acid battery SOH representative characteristics, often appear nonlinear to battery usable capacity throughout the battery service life. Therefore, to estimate the battery SOH from a change of battery usable capacity during the entire lead-acid battery service life, besides considering the battery SOH characteristics, additional testing methods must be imposed in order to improve SOH estimation accuracy.

* Corresponding author. Tel.: +886 4 2392 4505x7272; fax: +886 4 2392 2156.

E-mail addresses: chaokh@ncut.edu.tw, chaokh0706@yahoo.com.tw (K.-H. Chao).

Therefore, this study conducts multiple lead-acid battery charging/discharging tests to propose a modified recognition structure based on extension theory (Cai, 1983), so that battery SOH recognition can be more accurate. Input characteristics for the proposed estimation approach include coup de fouet plateau voltage of lead-acid battery, internal resistance under lead-acid battery floating charge, and the ratio of these two characteristics (i.e., coup de fouet voltage plateau value/battery internal resistance, called transient current). By computing the correlation degree of these three characteristics with lead-acid battery usable capacity, this study can improve the estimation accuracy of the lead-acid battery life. It also references a recognition system based a neural network training mechanism from previous literature, takes absolute mean error between training data and recognition results for adjustment basis to expand/reduce the classic field of extension matter-element model, and further modify recognition results to meet the objective of the training data, and achieve the optimum estimation accuracy.

2. State-of-health characteristics of lead-acid batteries

Coup de fouet voltage is a kind of transient phenomenon, when discharging a fully-charged lead-acid battery, battery terminal voltage would fall instantaneously at initial discharge period, and thereafter restore to normal load voltage. As shown in Fig. 1, the minimal voltage during transient response to coup de fouet voltage is called trough voltage, and after trough voltage appears, battery discharge voltage will restore to discharge voltage in loading; battery terminal voltage at this time is called plateau voltage.

The most significant indicator of lead-acid battery SOH is usable capacity. Based on a knowing of usable capacity, one can further estimate remaining charging/discharging cycles or sustainable floating charge time of a lead-acid battery. According to previous literature, lead-acid battery SOH can be categorized in terms of five characteristics, operating temperature, internal resistance, floating voltage, floating current, and coup de fouet voltage. When choosing lead-acid battery SOH estimation characteristics, the following major factors are taken into account.

2.1. Refrain from prolonged monitoring of equipment

To users, battery SOH does not require real-time estimation, but the use of the Coulometric measurement method or prolonged monitoring of battery operating temperature requires more memory capacity of the estimation system, which benefit neither hardware volume nor cost, and prolonged estimation would impact on battery use.

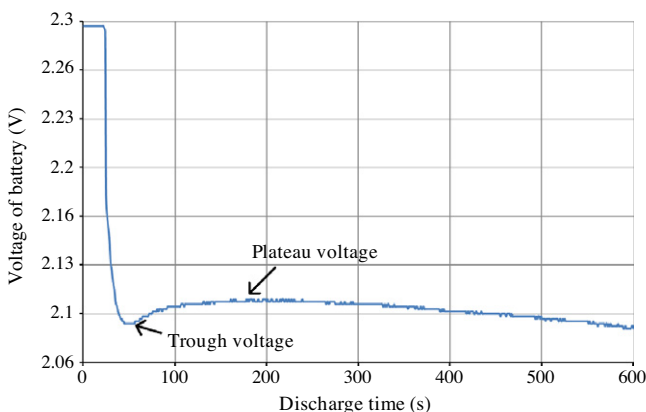


Fig. 1. Test curve of coup de fouet voltage for a lead-acid battery.

2.2. Restriction of estimation circuit hardware

As the relationship between lead-acid battery SOH and usable capacity is a nonlinear function, more characteristics are normally required to estimate its usable capacity in order to improve accuracy. However, the more characteristics used, the more complicated the estimation system, the higher the cost, and the more restrictions in application. Therefore, how to use the fewest estimation apparatus to achieve highly accurate SOH estimation remains a critical research topic.

2.3. Adaptiveness of estimation approach

Usable capacity of lead-acid battery can act as a uniform indicator for both battery floating life and recycle life. However, battery floating or recycling uses variable charging/discharging methods, therefore, if estimating SOH using a constant program testing method while satisfying both battery application modes, then the estimation approach would be more widely applied.

Based on the above factors, it is a good choice to select coup de fouet voltage as the major characteristic for estimating lead-acid battery SOH. The reason that coup de fouet voltage failed to estimate lead-acid battery SOH previously is that its variation is little, thus, error factors were too much. In other words, almost any kind of battery application environment factor, such as current floating voltage, previous depth of discharge, charging/discharging current and post-charge waiting time, could all cause measurement errors. In the implementation of a measuring system, a 10 mV scaled meter and a timekeeping device can measure coup de fouet voltage, except that the constant current discharge is difficult on a battery. Considering the influences of various factors on coup de fouet voltage, this study performs 10% and 100% depth discharge on a 12V-13Ah lead-acid battery, respectively, and adopted a 0.1 C current to charge the lead-acid battery, allowing the charge voltage to reach 15.2 V and floating charge, then measured internal battery resistance and floating voltage after 120 min waiting time, followed by a 0.5 C current to discharge the battery for 10 min in order to acquire its coup de fouet voltage data. The general test system structure is shown in Fig. 2, where a programmable system on chip (PSoC) microcontroller is the control kernel of the entire system

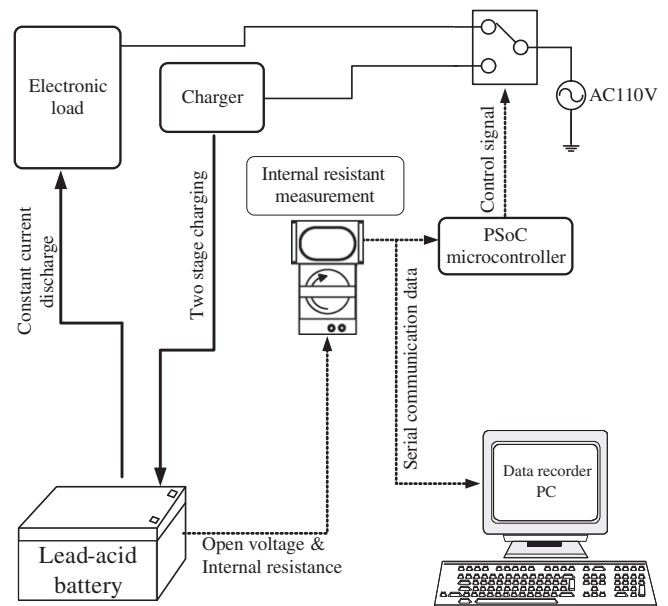


Fig. 2. Scheme of lead-acid battery coup de fouet voltage acquisition system.

(Technical Reference Manual for All PSoC Devices with a Base Part Number of CY8C2, XXXX), PSoC governs the battery power supply to the electronic load for 0.5 C constant current discharge, or charges battery by means of dual level constant current charging. A battery tester monitored terminal voltage and internal resistance of the lead-acid battery in real time, and transferred the information to a PSoC microcontroller and personal computer for data storage. From the battery terminal voltage, as acquired by the battery tester, the PSoC microcontroller can determine whether the battery is fully charged and should go to waiting time, or the discharge has finished and the battery should be recharged.

General charging/discharging behavior of the testing system is shown in Fig. 3, according to changes in the battery terminal voltage, testing system operations can be divided into three stages. The first is a charging stage, when the battery charger is begun to perform a constant current charging of the battery by means of a dual stage charge, where the charge current is set at 0.1 C (about 1.3 A). After the battery charge voltage rises to 15.2 V, the system goes into a waiting state, while continuing to supply 13.8 V of floating charge voltage to the battery. The battery waiting time is set at 120 min. Thereafter, a counter in the PSoC microcontroller generates an interruption signal to end the charging action, and starts an electronic load to perform constant current discharging of the battery, which is set at a 0.5 C (about 6.5 A) discharge current to test coup de fouet voltage; experimental results proved that this test procedure can obtain a more significant coup de fouet voltage. Finally, after discharging for 10 min at a constant current, the Coulometric measurement method is used to compute the power consumption in battery.

As known from specifications provided by battery manufacturers, in cases of 100% depth of discharge, the lead-acid battery recycle life can maintain at least 200 charging/discharging cycles. Therefore, to speed battery aging and facilitate observations, this study carries out multiple cycles of in-depth large current discharge and rapid large current charging of batteries, throughout a battery's life with a discharge current of 1 C (13 A), which persisted until a 5 V cutoff voltage; and a charge current of 0.5 C (6.5 A), charging to a 15.2 V saturation voltage, followed by observations of changes in battery discharge time during aging. According to the Coulometric measurement method, a significantly decreased battery discharge time indicates that battery usable capacity is varied. Next, characteristic value acquisition tests are run on the coup de fouet voltage, as mentioned above. Fig. 4 shows the flow chart of battery aging tests. Throughout an entire battery life, 14 coup de fouet voltage measurement tests are employed, with the Coulometric measurement method running battery usability capacity tests. Fig. 5 shows the test curve of battery usable capacity versus coup de fouet plateau voltage. Fig. 6 shows

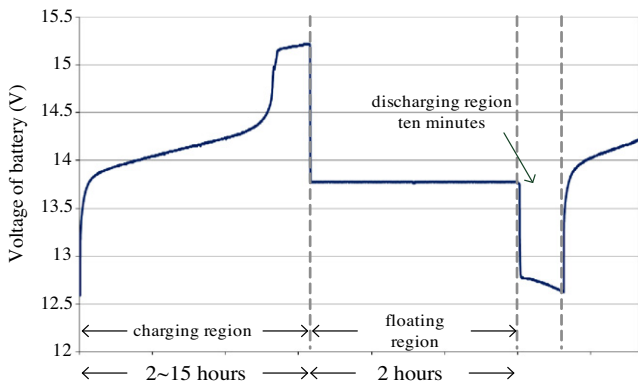


Fig. 3. Change of battery terminal voltage during coup de fouet voltage acquisition.

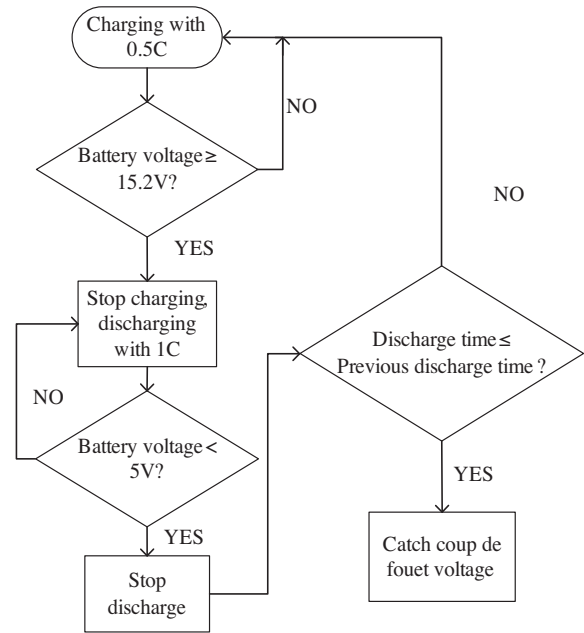


Fig. 4. Flow chart of the battery aging test.

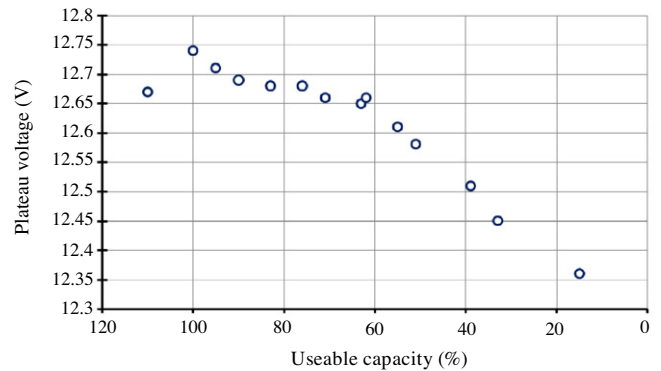


Fig. 5. Test curve of coup de fouet plateau voltage versus usable capacity of lead-acid battery.

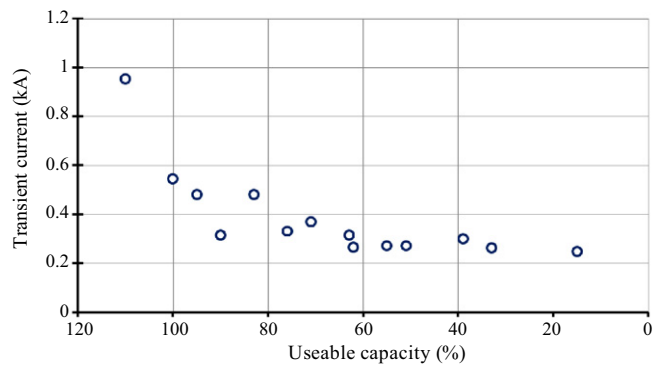


Fig. 6. Test curve of transient current versus usable capacity of lead-acid battery.

the test curve of battery usable capacity versus battery transient current. Fig. 7 shows the test curve of battery usable capacity versus battery internal resistance in the floating stage. As shown in Figs. 5–7, compared with other characteristics, the relation between coup de fouet plateau voltage and battery usable capacity

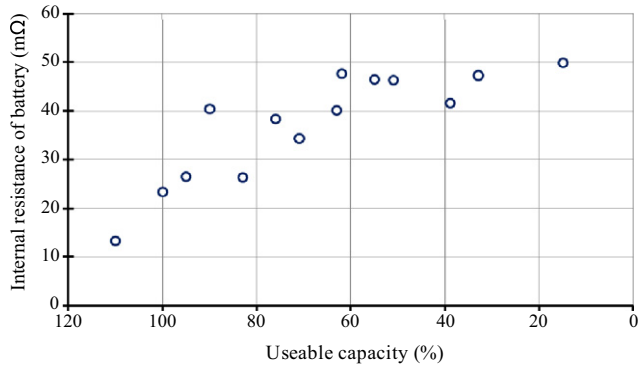


Fig. 7. Test curve of internal resistance versus useable capacity of lead-acid battery.

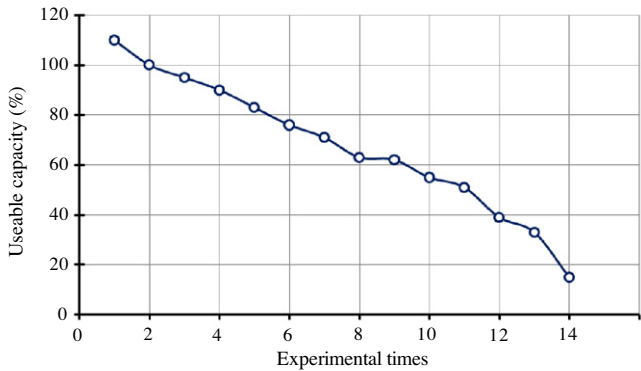


Fig. 8. Data distribution of 14 tests on useable capacity over battery service life.

is the most linear. Therefore, if using coup de fouet plateau voltage as the main characteristic of estimating lead-acid battery SOH, higher estimation accuracy should be attained.

Among 14 tests of usable capacity throughout a lead-acid battery’s service life, the capacity results shown in Fig. 8 have a continuous descending function with increased use time and charging/discharging cycles. To facilitate computing and comparison of estimation results, percentage% is universally used in this study to represent battery usable capacity, that is, the rated capacity (e.g., 10 Ah) marked by the battery manufacturer is deemed 100% of the usable capacity. If total discharge results in half of original rated capacity (5 Ah) after battery aging, then the usable capacity is deemed as 50%. If using such usable capacity percentage to represent lead-acid battery SOH, then battery usable capacity test results would be between 10% and 110% in any category of battery SOH.

3. Modified recognition structure based on extension theory

If phenomena of life are referred to as the “matter”, to differentiate the matters, they must be named. Each matter has its corresponding characteristics, and these characteristics have corresponding values; therefore, elements describing a matter include the matter name, characteristic, and characteristic value. In the extension theory (Cai, 1983), these three basic elements constitute a matter-element, composed of *N* (name), *C* (characteristic), and *V* (value of characteristic) of any given matter, thus, a matter-element mathematical formula can be expressed as in (1)

$$R = (N, C, V). \tag{1}$$

According to the relation between matter-element, characteristic, and value, $V = C(N)$, (1) can be expressed as:

$$R = (N, C, C(N)). \tag{2}$$

According to the matter-element theory, the matter-element itself not only has a single characteristic, as shown in (1), if the matter-element contains an *n*-dimensional characteristic vector $C = [C_1, C_2, \dots, C_n]$, then the corresponding characteristic vector should be expressed as $V = [V_1, V_2, \dots, V_n]$. As shown in (3), the state-of-health of a 12 V–13 Ah lead-acid battery, as studied in this paper, is represented by a matter-element model, the matter name is battery life or usable capacity%, the characteristic vector is [*C*₁: coup de fouet plateau voltage $V_{plateau}$, *C*₂: internal resistance R_{in} , *C*₃: instantaneous current ($V_{plateau}/R_{in}$)], and the corresponding characteristic vector values are [12.74 V, 40.38 mΩ, 1.02 kA]. Fig. 9 is an illustration of the matter-element combination characteristics represented in 3D space, where matter name *N*, characteristic *C*, and value *V* correspond to *x*, *y*, *z*-axes, respectively, each combination is represented in space coordinates, and the three axes are extended to the matter-element space

$$R = (N, C, V) = \begin{bmatrix} N & C_1 & V_1 \\ & C_2 & V_2 \\ & C_3 & V_3 \end{bmatrix} = \begin{bmatrix} \text{Usable capacity \%} & V_{plateau} & 12.74 \text{ V} \\ & R_{in} & 40.38 \text{ m}\Omega \\ & V_{plateau}/R_{in} & 1.02 \text{ kA} \end{bmatrix}. \tag{3}$$

In practice, the application of the extension theory should be realized by an appropriate mathematical tool. The extension evaluation method is based on two terms, an “extension set” and the “correlation function,” which are applied with practical estimation rules (Cai, 1983). Its main idea is to divide matter into some category sets, which are determined according to data accumulated in various experiments, and then allow a database or an expert to comment on the data range of each category set, and then substitute the assessment data into each category data range in order to compute the correlation degree. Evaluated results are compared in terms of correlation degree of each category set, the greater the correlation degree, the greater consistency of the assessment data in the category sets. The specific evaluation steps are as follows:

Step 1: Define classical field and joint field.

If matter *R* can be divided into *j* categories, denoted by R_j , and *n* characteristic matrices *C* represent this matter, then, the characteristic spread is called X_p , and *P* is the defined set in all characteristic spreads in *j* categories, X_{pi} can be defined as all probable numerical

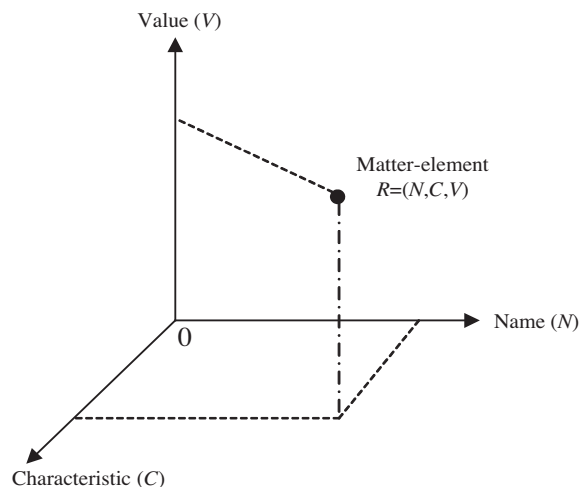


Fig. 9. Illustration of matter-element space.

ranges arising from each i th characteristic, and a_{pi} and b_{pi} , respectively, denote the probable maximum and minimum numerical ranges arising from each i th characteristic. Hence, the joint field R_p of such matter can be defined as shown in (4)

$$R_p = (P, \mathbf{C}, \mathbf{X}_p) = \begin{bmatrix} P & C_1 & X_{p1} = \langle a_{p1}, b_{p1} \rangle \\ & C_2 & X_{p2} = \langle a_{p2}, b_{p2} \rangle \\ & \vdots & \vdots \\ & C_n & X_{pn} = \langle a_{pn}, b_{pn} \rangle \end{bmatrix}. \quad (4)$$

In joint fields, numerical sets with matter R divided into j categories, are called classical fields, where N_j represents the individual characteristic range of the j category sets, C_i denotes the i th characteristic of this category, X_{ji} denotes the input data spread of the i th characteristic in the j th category, and a_{ji} and b_{ji} represent the maximum and minimum of this characteristic input of the j categories, respectively, this range is defined as the classical field of the i th characteristic in the j th category. Where, Y_{ji} is the output data spread of the i th characteristic in the j th category, and c_{ji} and d_{ji} represent the maximum and minimum of this characteristic output in this category, respectively, thus, it is deemed as an output classical field of testing data. Hence, the j th classical field R_j is defined for this matter, thus, a matter R can be divided into joint field R_p and j classical fields R_j , as shown in (5)

$$R_j = (\mathbf{N}_j, \mathbf{C}, \mathbf{X}_j, \mathbf{Y}_j) = \begin{bmatrix} N_j & C_1 & X_{j1} = \langle a_{j1}, b_{j1} \rangle & Y_{j1} = \langle c_{j1}, d_{j1} \rangle \\ & C_2 & X_{j1} = \langle a_{j1}, b_{j1} \rangle & Y_{j1} = \langle c_{j1}, d_{j1} \rangle \\ & \vdots & \vdots & \vdots \\ & C_n & X_{jn} = \langle a_{jn}, b_{jn} \rangle & Y_{jn} = \langle c_{jn}, d_{jn} \rangle \end{bmatrix} \quad (5)$$

Taking the curve of coup de fouet plateau voltage versus usable battery capacity, shown in Fig. 5, as an example; when battery usable capacity falls from 90% to 100%, the relationship between usable capacity and plateau voltage is linear. Therefore, according to (5), plateau voltage range is set within the interval of (12.69–12.74 V), and denote the upper bounds and lower bounds of classical field X_{11} , at the input end of category R_1 (i.e., battery usable capacity input data spread of the 1st characteristic in the 1st category), and sets the corresponding usable capacity range of (90–100%) as the upper bounds and lower bounds of classical field Y_{11} , at output end of category R_1 . In Fig. 5, four categories of classical fields (i.e., divided into four linear regions) are built according to linearity between usable battery capacity and plateau voltage, the plateau voltage at 110% usable battery capacity is even lower than that at 90% usable capacity. Then, if classifying 110% usable capacity as category R_1 , the input ends of classical fields category R_1 and category R_2 will overlap, leading to estimation errors; thus, it is more appropriate to classify it as category R_2 , according to the plateau voltage at 110% usable capacity. According to (5) and numerical spread linearity, the above three characteristics can be built into an extension matter-element model, where joint field R_p , input classical field X_{ji} ,

and output classical field Y_{ji} , of each characteristic, are listed in Table 1, respectively.

Step 2: Determine assessment matter-elements.

A group of characteristic values within matter-element R is called assessment matter-element of matter R ; if this matter-element has n characteristics, then this matter-element can be represented by:

$$R = (q, \mathbf{C}_i, \mathbf{x}_i) = \begin{bmatrix} q & C_1 & x_1 \\ & \vdots & \vdots \\ & C_i & x_i \\ & \vdots & \vdots \\ & C_n & x_n \end{bmatrix}, \quad (6)$$

where, q denotes this group of characteristic values, and x_i denotes the value of C_i , and the i th characteristic of q , or specific data obtained from tests of assessment matter, thus, matter R can have multiple groups of characteristic q values.

Step 3: Determine weighting factor.

The importance of each characteristic C_i to matter R is called the weighting factor w_i ; which is expressed by a value of 0–1, according to its importance, and the sum is 1, that is:

$$\sum_{i=1}^n w_i = 1. \quad (7)$$

Step 4: Determine correlation degree of assessment data of each category.

3.1. Computing distance

Distance refers to the difference between the distance of one characteristic value x_i , taken from the center point of joint field R_p of this characteristic (or each classical field R_j), and the distance from center of gap between the upper and lower bounds of the joint field R_p (or classical field R_j); therefore, the distance of characteristic value x_i from joint field R_p can be defined as:

$$\rho(x_i, X_{pi}) = \left| x_i - \frac{a_{pi} + b_{pi}}{2} \right| - \frac{b_{pi} - a_{pi}}{2}. \quad (8)$$

The distance of the characteristic value x_i from each classical field R_j is defined as:

$$\rho(x_i, X_{ji}) = \left| x_i - \frac{a_{ji} + b_{ji}}{2} \right| - \frac{b_{ji} - a_{ji}}{2}. \quad (9)$$

3.2. Computing correlation function

After computing distance, the correlation function can be computed; the correlation function $k_j(x_i)$ depicts the membership of each characteristic of assessment matter q with respect to assessment category j . The computational method of correlation function $k_j(x_i)$, listed in (10), contains the initial classification of the test data; or, if the classical field distance calculated from (9), is greater than 0, then it indicates that the test data are not completely within the range of this state-of-health (SOH). In cases where the joint field distance is the same as the distance of the classical field, it indicates that the correlation function value approximates to infinity, and cannot be resolved; however, the correlation function for this case, and the case of a classical field distance below 0, can be computed. After computing the correlation function of the test-

Table 1
Matter-element model of lead-acid battery at variable state-of-health.

R_1	C_1	(12.69, 12.74)	(90, 100)	R_2	C_1	(12.64, 12.67)	(62, 110)
	C_2	(13.13, 40.38)	(83, 110)		C_2	(27.40, 41.21)	(63, 90)
	C_3	(0.38, 1.02)	(83, 110)		C_3	(0.32, 0.47)	(71, 76)
R_3	C_1	(12.58, 12.66)	(51, 63)	R_4	C_1	(12.36, 12.51)	(15, 39)
	C_2	(46.16, 47.46)	(51, 55)		C_2	(40.13, 48.47)	(15, 62)
	C_3	(0.258, 0.307)	(39, 90)		C_3	(0.25, 0.304)	(15, 62)
R_p	C_1	$X_{p1} = \langle 12.36, 12.74 \rangle$					
	C_2	$X_{p2} = \langle 13.13, 48.47 \rangle$					
	C_3	$X_{p3} = \langle 0.25, 1.02 \rangle$					

ing data through (10), the correlation function $K_j(x_i)$ of each characteristic, for each category of test data, can be obtained:

$$k_j(x_i) = \begin{cases} \frac{-\rho(x_i, X_{ji})}{|X_{ji}|} & , \rho(x_i, X_{ji}) = \rho(x_i, X_{pi}) \\ & \text{or } \rho(x_i, X_{ji}) < 0 \\ \frac{-\rho(x_i, X_{ji})}{\rho(x_i, X_{ji}) - \rho(x_i, X_{pi})} & , \rho(x_i, X_{ji}) \neq \rho(x_i, X_{pi}) \end{cases} \quad (10)$$

Using the extension correlation function formula in (10) to compute the correlation function of each characteristic value x_i of this matter-element, the relationship between characteristic value x_i and extension correlation function $k_j(x_i)$ is shown in Fig. 10. As seen, when the characteristic value is nearer the center point of classical field R_j , then the obtained correlation function $k_j(x_i)$ is more approximate to 1, and if the characteristic value is not within the classical field range, the derived correlation function will be negative. Therefore, in the structure of the extension theory, the correlation function $k_j(x_i)$ indicates the degree of each characteristic value belong to an interval.

If expanding number of classical field of this matter R_j to m , then classical field of this matter can be represented by

$$R_m = (N_m, C, X_m = \langle a_m, b_m \rangle). \quad (11)$$

Similarly, using (10) to depict the relationship between the characteristic value and the correlation function of each classical field as shown in Fig. 11. As seen, characteristic value x_i produces the correlation function $k_j(x_i)$ for each classical field X_j , and every correlation function $k_j(x_i)$ varies with the distance of characteristic value x_i , as taken from the center of classical field X_j . According to the correlation function value, the extension theory determines the correlation degree between each output category j and input characteristic value x_i .

The mapping relationship between input characteristic data x_i and output category j is shown in Fig. 12, where the columns in 3D space represent the relationship between input characteristic x_i , output category j and correlation function $k_j(x_i)$. Input characteristic x_i on axis-X and output category j on axis-Y form the X-Y

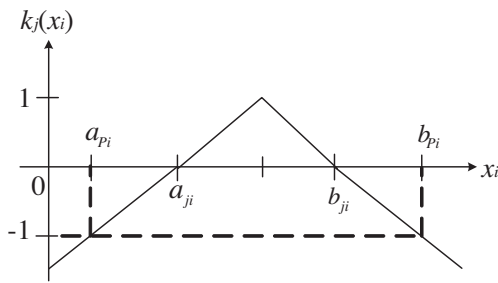


Fig. 10. Relationship curve of characteristic value versus correlation function.

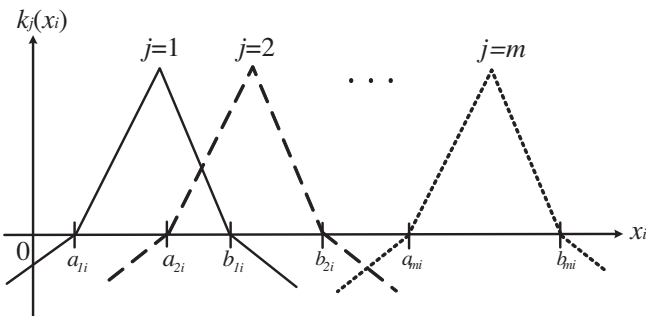


Fig. 11. Relationship between characteristic value x_i and m categories of correlation functions.

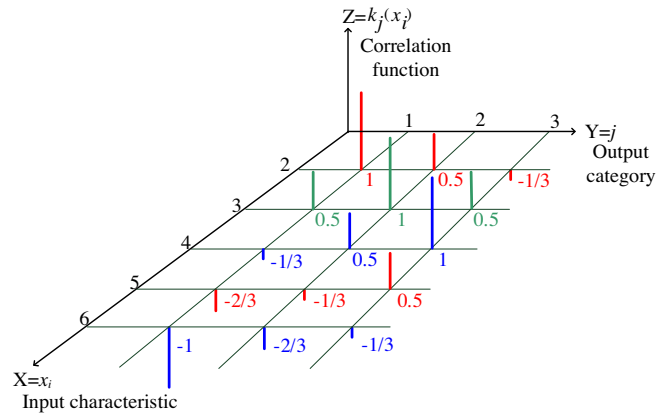


Fig. 12. Column diagram formed by plane of characteristic value x_i versus j categories and correlation function.

plane, the axis-Z vertical to the plane represents corresponding correlation function $k_j(x_i)$ for each point on X-Y plan. The X-Z display is according to the curve of input characteristic data versus the correlation function, as shown in Fig. 11. In Fig. 12, matter-element is divided into three categories (or $j = 3$), if there is only one characteristic, then matter-element model is represented by:

$$\begin{aligned} R_1 &= (N_1, C_1, X_{11} = (1, 3)), \\ R_2 &= (N_2, C_1, X_{21} = (2, 4)), \\ R_3 &= (N_3, C_1, X_{31} = (3, 5)), \\ R_p &= (P, C_1, X_p = (0, 6)). \end{aligned} \quad (12)$$

When input x_i is 2, the obtained three categories of correlation function values $k_j(x_i)$ will be:

$$k_1(2) = 1, \quad k_2(2) = 0.5, \quad k_3(2) = -1/3. \quad (13)$$

Similarly, when input x_i is 4, the obtained three categories of correlation function values $k_j(x_i)$ will be:

$$k_1(4) = -1/3, \quad k_2(4) = 0.5, \quad k_3(4) = 1. \quad (14)$$

If x_i is 2, the drawn curve of Y-Z plane will be shown in Fig. 13, as known from comparisons with Fig. 11, j categories of a matter can generate j -dimensional extension correlation function $k_j(x_i)$, and by mapping this j -dimensional extension correlation function, a two-dimensional space can be obtained based on category j . In the conventional extension theory, the basis j for the maximum correlation function value in such 2D space is regarded as the estimated category. Further study of the curve of input on axis-X (characteristic) versus output on axis-Y (category), as shown in Fig. 12, finds that as input x_i on axis-X changes, the mapped output on axis-Y also varies continuously with correlation function $k_j(x_i)$. Therefore, if giving a data range for an output end category, then the estimated output category can be computed from correlation

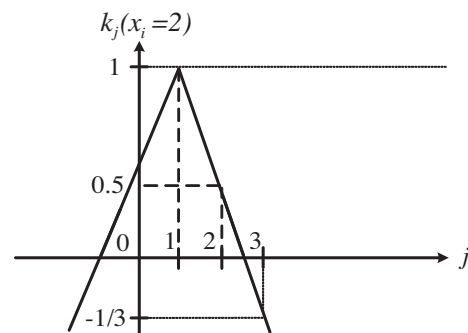


Fig. 13. Relationship between correlation function and matter-element category j .

function $k_j(x_i)$, as shown in Fig. 13, and obtain continuous output category estimations, which vary with input data. If there are multi-dimensional characteristics in the matter-element, then the correlation function for each characteristic can be obtained by the same method as above. From the value of the correlation function of each characteristic, the estimation of each corresponding output category can be computed.

Step 5: Compute the correlation degree.

The computed correlation function $k_j(x_i)$ is multiplied by the weight of the characteristic with respect to category, and summed to obtain a correlation degree of each assessment category, λ_j . Then, from (15), obtain category j attributed to the maximum correlation degree for test data categories, such category is the assessment result of the conventional extension theory (Cai, 1983)

$$\max(\lambda_j) = \max \left(\sum_{i=1}^n w_i \times k_j(x_i) \right), \quad j = 1, 2, \dots, m. \quad (15)$$

To make the output estimation result continuous, as shown in Fig. 10, if the characteristic value is nearer the center point of the classical field, then its correlation function is more approximate to 1. Therefore, by using the center point of classical field Y_{ji} , at the output end and range of classical field Y_{ji} in (5), then more definite output values can be computed from each category of correlation function $k_j(x_i)$. The correlation function of the output layer can be derived from the maximum correlation function 1 minus category correlation function $k_j(x_i)$, and that can be expressed as:

$$k_j^{out}(x_i) = 1 - k_j(x_i). \quad (16)$$

After the computation of (16), the relationship between the output category and the output layer correlation function $k_j^{out}(x_i)$ is shown in Fig. 14. The value of category j corresponding to mini-

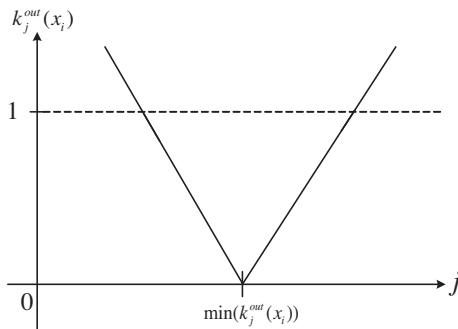


Fig. 14. Relationship curve of output layer correlation function versus matter-element category j .

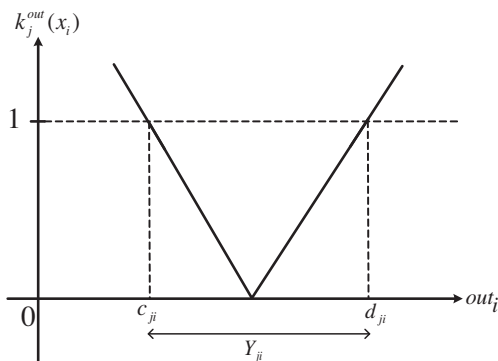


Fig. 15. Relationship curve of output layer correlation function versus output classical field.

um of the derived output layer correlation function $k_j^{out}(x_i)$ acts as a basis of output computation. By computing the output range by (17), the explicit output data out_i can be obtained. The curve of the output layer correlation function $k_j^{out}(x_i)$ versus the data range of output category j , as shown in Fig. 15

$$out_i = \left(\frac{c_{ji} + d_{ji}}{2} \right) \pm \frac{d_{ji} - c_{ji}}{2} \times k_j^{out}(x_i) \times \frac{v}{|v|}, \quad (17)$$

where $v \triangleq x_i - \frac{a_{ji} + b_{ji}}{2}$ is the distance of the test data from the center point of the classical field, and the symbol “ \pm ” in (17) can be determined by the slope of a linear equation derived from testing data versus the usable capacity curve by the first order of linear regression. If a matter possesses n characteristics, then the estimation result of each characteristic obtained from (17) can be multiplied by the weighting factor of (7), and then summed to obtain the recognition results in (18)

$$out = \sum_{i=1}^n w_i \times out_i. \quad (18)$$

4. Extension evaluation method with learning mechanism

To improve the lead-acid battery SOH estimation accuracy, this paper proposes an extension supervised training system with a learning mechanism, as shown in Fig. 16. The recognition structure in Fig. 16 only shows the i th characteristic C_i of the j th category matter-element R_j , where the input classical field range is $X_{ji} = \langle a_{ji}, b_{ji} \rangle$, while the output classical field range is $Y_{ji} = \langle c_{ji}, d_{ji} \rangle$. The curve of characteristic C_i input, in , versus the output estimation, out_i^t , is as shown on the top left of Fig. 16. In the center of the figure, characteristic C_i input, in , changes from 0 to ∞ , and the curve of the input data versus correlation function $k_{ji}(in)$ is derived from (10). The top right of the figure is the curve of the output layer correlation function $k_{ji}^{out}(in)$, versus output category numerical range Y_{ji} , and obtained from (16) and (17). If input in is exactly equal to a_{ji} or b_{ji} , then output out_{ji} , after recognition in (17), will be c_{ji} and d_{ji} . In this paper, training data is represented by $T = \{T_1, T_2, \dots, T_{np}\}$, where np is the total of the training data, thus, the matter-element model for the i th training data can be defined as:

$$T_i = (out_i, C_i, X_i^t) = \begin{bmatrix} out_i^t & C_1 & x_1^t \\ & C_2 & x_2^t \\ & \vdots & \vdots \\ & C_n & x_n^t \end{bmatrix}, \quad i = 1, 2, \dots, np \quad (19)$$

where out_i^t is the known output of the said training data of the supervised learning procedure, and C_i is the matrix of the n characteristics of the matter-element, and X_i^t is the value of C_i for n characteristics of the training data. After building the matter-element model in Table 1 through (5), we can train according to the proposed structure, and further adjust the output classical field till optimum. The adjustment procedure is, input the i th training data into the recognition structure of Fig. 16, and compare recognition results out_i with the known would-be out_i^t to obtain recognition error e , then, adjust the classical field of output Y_{ji} , in order that $out_i^t = out$. An example is presented below to describe the learning procedure of the supervised training system constructed by this study; suppose two training data, T_1 and T_2 , are defined as:

$$\begin{aligned} T_1 &= (out_1, C_1, x_1^t) = (c + 1, C_1, a), \\ T_2 &= (out_2, C_1, x_1^t) = (d, C_1, b), \end{aligned} \quad (20)$$

where T_2 input $x_1^t = b$, and from the recognition structure shown in Fig. 16, the result is estimated as $out_2 = d$, and is compared with known output T_2 $out_2^t = d$, to obtain error $e = out_2 - out_2^t = 0$. Regard-

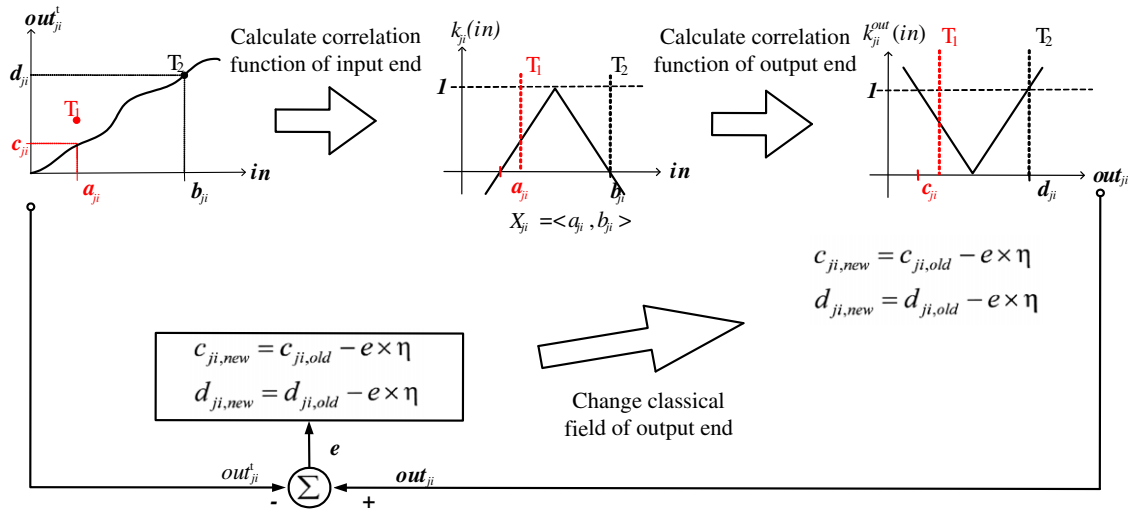


Fig. 16. Scheme of extension supervised training procedure with a learning mechanism.

ing T_1 input $x_1^t = a$, it is estimated from the recognition structure in Fig. 16 to obtain $out_1 = c$, and then the known output of T_1 , $out_1^t = c + 1$, is compared to obtain its error $e = 1$. Multiplying this error e by the learning rate (η), and adjusting through (21), to adjust the classical field output range Y_{11} , and further changes the output estimation

$$c_{ji,new} = c_{ji,old} - e \times \eta$$

$$d_{ji,new} = d_{ji,old} - e \times \eta. \tag{21}$$

Adjustment of output classical field in training is shown in Fig. 17. Because error $e = 1$ for recognition result of training data T_1 , lower bound of the output classical field is adjusted by (21). The training system calculates a new lower bound for output classical field $c_{ij,new} = c + 1$, therefore, the final recognition result of training data T_1 is, $out_1 = c + 1 = out_1^t$, where output error $e = 0$. It indicates that the output has been changed to the known output of the training data by adjusting the output classical field. Finally, repeat input training data into the training procedure until output recognition results are obtained for all training data, out_i , thus, meeting its target out_i^t , then the (21) derived output classical field range will no longer be changed, indicating that the recognition result has been optimized at this time. Fig. 18 shows the curve of input in versus the estimated output out , both before and after training procedures are completed. The corresponding recognition result of input of training data T_1 has been changed from the original c to $c + 1$ after the training procedure, and the recognition error

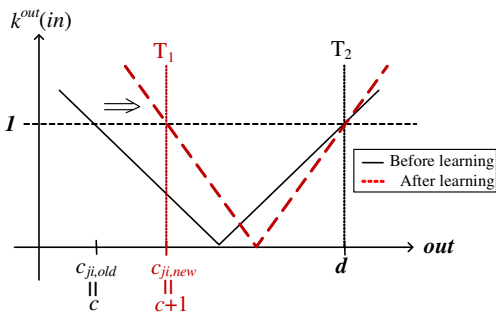


Fig. 17. Illustration of output classical field adjustment during training.

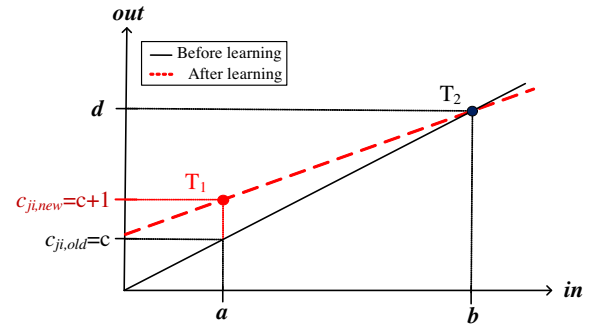


Fig. 18. Curve of input versus output in recognition structure before and after training.

e falls from 1 to 0. It indicates that the output classical field range Y_{11} , and its corresponding training data, are optimized after training procedure adjustments.

Therefore, according to the definition of the matter-element theory, (19) can be used to represent 14 sets of training data built from the characteristic data of a lead-acid battery in various SOH,

Table 2
14 sets of training data on lead-acid battery SOH built on experiment.

T_1	$\begin{bmatrix} 110 & C_1 & x_1^t = 12.67 \\ & C_2 & x_2^t = 13.29 \\ & C_3 & x_3^t = 0.953 \end{bmatrix}$	T_2	$\begin{bmatrix} 100 & C_1 & x_1^t = 12.74 \\ & C_2 & x_2^t = 23.37 \\ & C_3 & x_3^t = 0.545 \end{bmatrix}$	T_3	$\begin{bmatrix} 95 & C_1 & x_1^t = 12.71 \\ & C_2 & x_2^t = 26.49 \\ & C_3 & x_3^t = 0.479 \end{bmatrix}$
T_4	$\begin{bmatrix} 90 & C_1 & x_1^t = 12.69 \\ & C_2 & x_2^t = 40.54 \\ & C_3 & x_3^t = 0.313 \end{bmatrix}$	T_5	$\begin{bmatrix} 83 & C_1 & x_1^t = 12.68 \\ & C_2 & x_2^t = 26.38 \\ & C_3 & x_3^t = 0.48 \end{bmatrix}$	T_6	$\begin{bmatrix} 76 & C_1 & x_1^t = 12.68 \\ & C_2 & x_2^t = 38.4 \\ & C_3 & x_3^t = 0.33 \end{bmatrix}$
T_7	$\begin{bmatrix} 71 & C_1 & x_1^t = 12.66 \\ & C_2 & x_2^t = 34.44 \\ & C_3 & x_3^t = 0.367 \end{bmatrix}$	T_8	$\begin{bmatrix} 63 & C_1 & x_1^t = 12.65 \\ & C_2 & x_2^t = 40.19 \\ & C_3 & x_3^t = 0.314 \end{bmatrix}$	T_9	$\begin{bmatrix} 62 & C_1 & x_1^t = 12.66 \\ & C_2 & x_2^t = 47.74 \\ & C_3 & x_3^t = 0.265 \end{bmatrix}$
T_{10}	$\begin{bmatrix} 55 & C_1 & x_1^t = 12.61 \\ & C_2 & x_2^t = 46.57 \\ & C_3 & x_3^t = 0.27 \end{bmatrix}$	T_{11}	$\begin{bmatrix} 51 & C_1 & x_1^t = 12.58 \\ & C_2 & x_2^t = 46.44 \\ & C_3 & x_3^t = 0.27 \end{bmatrix}$	T_{12}	$\begin{bmatrix} 39 & C_1 & x_1^t = 12.51 \\ & C_2 & x_2^t = 41.66 \\ & C_3 & x_3^t = 0.3 \end{bmatrix}$
T_{13}	$\begin{bmatrix} 33 & C_1 & x_1^t = 12.45 \\ & C_2 & x_2^t = 47.4 \\ & C_3 & x_3^t = 0.262 \end{bmatrix}$	T_{14}	$\begin{bmatrix} 15 & C_1 & x_1^t = 12.36 \\ & C_2 & x_2^t = 50 \\ & C_3 & x_3^t = 0.247 \end{bmatrix}$		

Table 3
Optimal training learning rate for each characteristic.

	C ₁ : Plateau voltage	C ₂ : Internal resistance	C ₃ : Transient current
Average absolute error (before training)	8.2%	11.3%	12.38%
Best learning rate (η)	3.4	1.07	3.36
Average absolute error (after training)	4.03%	8.02%	7.5%
Convergence times of learning error	1	4	2

and details of each set of data are listed in Table 2. Then, these 14 sets of test data are inputted into the training procedure, and train classical field Y_{ji} for three output characteristics. The general structure of the training procedure is shown in Fig. 16, where (10) is used to compute the correlation function $k_j(x_i)$ of the j th category for the three characteristics of training data, respectively. And from (16) and (17), the output layer correlation function $k^{out}(x_i)$ can be computed to further know the value of output category out_i . Thus, by comparing characteristic output out_{ji} with the known output category of training data out_{ji}^t , their error e can be obtained, and by adjusting the output classical field range through (21), the estimation result of each characteristic out_{ji} is changed. The completion of one training cycle is indicated upon inputting the 14 sets of training data into the training procedure shown in Fig. 16. Nonetheless, in actual training procedures of a matter-element model, training data is repeatedly input into the training system, and training procedures will be stopped only when the estimation error of each characteristic e is less than the preset target, or the training cycles are more than the maximal preset number of cycles.

In (21), the output classical field of the matter-element model is adjusted. The estimating error e was used to determine the increase and decrease of the classical field. Nevertheless the learning rate η influences the output error convergence rate and estimation accuracy. A faster learning rate can speed the convergence of output errors, but estimation accuracy would decrease. Alternatively, a slower learning rate enables greater error convergence accuracy, but learning cycles and time will be greatly increased. Thus, the learning rate setting is another key factor of the training procedures. In this paper, there are 500 learning rates for each characteristic, learning rate η is scaled at 0.01, between 0 and 5. They are input into the proposed recognition structure for training. The mean absolute error of minimal estimation errors obtainable from the 14 sets of training data of each learning rate are recorded, and the mean absolute error me is defined as:

$$me = \frac{\sum_{i=1}^n |out_i - out_i^t|}{n} \quad (22)$$

Mean absolute errors, optimal learning rates, and error convergence rates obtained from the training data of the three characteristics, C₁

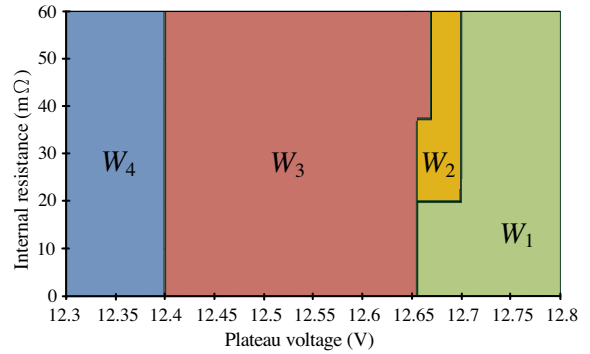


Fig. 19. Optimal weight combinations selected for plateau voltage and internal resistance in various regions.

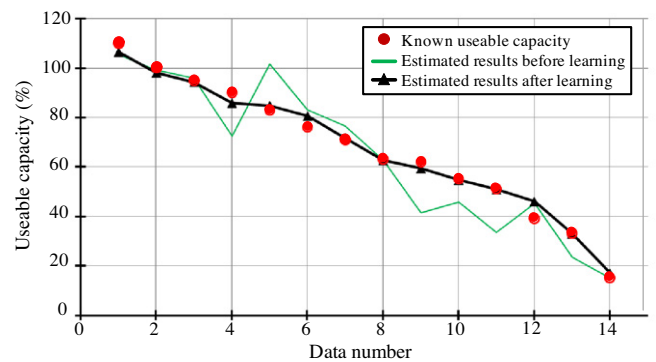


Fig. 20. Estimation result of lead-acid battery SOH before and after training.

(plateau voltage), C₂ (internal resistance), and C₃ (instantaneous current), are tabulated in Table 3. The matter-element model built after training, as shown in Table 4, as compared with the empirically built matter-element model in Table 2, recognition accuracy of the output classical field range has been greatly improved after appropriate adjustments.

After finishing training procedures of the matter-element model, and according to the test results of the training data, this study employed (18) to select one of four weighting factor combinations, as shown in (23), and chose one of the best four weights according to the spread of the test characteristic values of C₁ (plateau voltage) and C₂ (internal resistance), the ranges of the best four weights are shown in Fig. 19

$$\begin{aligned} W_1 &= \langle w_1 = 0.1, w_2 = 0.8, w_3 = 0.1 \rangle \\ W_2 &= \langle w_1 = 0.8, w_2 = 0.1, w_3 = 0.1 \rangle \\ W_3 &= \langle w_1 = 0.6, w_2 = 0.1, w_3 = 0.3 \rangle \\ W_4 &= \langle w_1 = 0.1, w_2 = 0.1, w_3 = 0.8 \rangle. \end{aligned} \quad (23)$$

Table 4
Matter-element model for lead-acid battery SOH estimation after training by a system with a learning mechanism.

R_1	$\begin{bmatrix} N_{01} & C_1 & (12.69, 12.74) & (90, 100) \\ & C_2 & (13.13, 40.38) & (78.2, 110) \\ & C_3 & (0.38, 1.02) & (90, 110) \end{bmatrix}$	R_2	$\begin{bmatrix} N_{02} & C_1 & (12.64, 12.67) & (63, 82.06) \\ & C_2 & (27.4, 41.21) & (74.7, 73.5) \\ & C_3 & (0.32, 0.47) & (71, 83) \end{bmatrix}$
R_3	$\begin{bmatrix} N_{03} & C_1 & (12.58, 12.66) & (51, 62) \\ & C_2 & (46.16, 47.46) & (51, 62) \\ & C_3 & (0.258, 0.307) & (55, 63) \end{bmatrix}$	R_4	$\begin{bmatrix} N_{04} & C_1 & (12.3, 12.51) & (15, 39) \\ & C_2 & (40.13, 48.4) & (36.2, 42.1) \\ & C_3 & (0.25, 0.30) & (15, 121) \end{bmatrix}$
R_p	$\begin{bmatrix} N_p & C_1 & X_{p1} = (12.36, 12.74) \\ & C_2 & X_{p2} = (13.13, 48.47) \\ & C_3 & X_{p3} = (0.25, 1.02) \end{bmatrix}$		

Table 5
Comparison of recognition errors of various estimation approaches at variable disturbing quantity.

Estimation method	Existed extension neural Network (Wang, 2003; Wang & Ho, 2005)			The proposed modified extension method with a learning mechanism		
Classical field numbers	4			4		
Data numbers	14	350	350	14	350	350
Random disturbance of joint field	±0%	±5%	±10%	±0%	±5%	±10%
Average absolute error (me)	9.07%	10.5%	11.91%	2.15%	5.95%	8.01%
Maximun error (e_{max})	35%	35%	60%	7.04%	20.45%	29.5%

Taking the characteristic data of 110% usable battery capacity as an example; as seen from Fig. 5, the plateau voltage of 110% usable battery capacity is 12.67 V; and as seen from Fig. 7, the battery internal resistance of 110% usable battery capacity is 13.29 mΩ. In the interval of 90–110% usable battery capacity, the curve of battery internal resistance versus usable capacity is more linear than the curve of plateau voltage versus usable capacity. Therefore, if estimating usable capacity from plateau voltage and internal resistance, respectively, the recognition error from internal resistance must be smaller, if giving greater weight w_2 to characteristic C_2 (internal resistance), or choosing W_1 in weight combinations from (23), then the accuracy of the estimation results derived from (18) must be higher. Therefore, when the plateau voltage input into the estimation program is greater than 12.67 V, we can see whether internal resistance is less than 20 mΩ to determine whether giving greater weight, W_1 (i.e., $w_1 = 0.1$, $w_2 = 0.8$, $w_3 = 0.1$), to characteristic C_2 (internal resistance), or giving greater weight, W_2 (i.e., $w_1 = 0.8$, $w_2 = 0.1$, $w_3 = 0.1$), to characteristic C_1 (plateau voltage). The estimation program can determine the weight combination according to the characteristics of test data, and the three characteristics adopted by the estimation program can be combined according to linearity with the estimation result, in order to improve general estimation accuracy.

According to (18), the estimation results of each characteristic are multiplied by their weight, and summed, thus, estimation results of the three characteristics can be combined to obtain the recognition result *out*. In this paper, the curve of the number of tests of the 14 sets of training data over an entire battery service life, versus the usable capacity, is drawn in Fig. 20, and estimation results of each group of data, both before and after training, are listed in the figure to facilitate comparison. In Fig. 20, the absolute mean error between the estimation results of the untrained matter-element model in Table 1 and test data is 8.43%, while the absolute mean error of estimation results of the trained matter-element model in Table 4 falls to 2.15%. Therefore, it proves that the training system proposed in this paper can optimize the training data matter-element model, and improve its recognition accuracy.

5. Test results of lead-acid battery SOH

To validate the recognition accuracy and robustness of the proposed lead-acid battery SOH estimation approach, according to the joint field range in the matter-element model, 5% and 10% disturbing quantity were added to the 14 sets of training data built in this study to obtain 350 sets of test data. The test data disturbing quantity is defined as:

$$x_i = x_i^t + rand \times (d_{pi} - c_{pi}) \times \langle 5\%, 10\% \rangle, \quad (24)$$

where “*rand*” represents the random function in $\langle -1, 1 \rangle$ made by random number generator, while d_{pi} and c_{pi} are the upper and lower bounds of the joint field of each matter-element model, respectively. According to the trained matter-element model in Table 4, (17) can be used to estimate usable battery capacity from 350 sets of test data under various disturbing quantities, and used (22) to compute absolute mean errors of the estimation results and usable

capacity of the known testing data, as listed in Table 5 for comparison. As shown in Table 5, when disturbing quantity of characteristic values is increased to $\pm 10\%$, the absolute mean error of the proposed modified extension method with a learning mechanism is about 8.01%, which is better than the 8.43% estimation accuracy of an untrained matter-element model. By setting an appropriate learning rate, the proposed method can greatly reduce training cycles, just four cycles of learning procedures; at most, can optimize the range of the matter-element model, giving it about $\pm 10\%$ noise resistance to input characteristic data. Hence, estimating the lead-acid battery SOH using a modified extension method with a learning mechanism proposed in this paper has better accuracy than other methods. And as the proposed approach applies a correlation function to map output values, the testing data classification categories become fewer, memory required for recognition system is reduced, thus, estimation rate is improved. As to results of recognition on the same test data, resulted from previously used extension neural network (ENN) recognition methods (Wang, 2003, 2005; Wang & Ho, 2005), as seen in Table 5, the existed extension neural network fails to output the respective input data continuously. Therefore, given the same amount of classical fields, recognition accuracy falls greatly by adopting the ENN method, especially in cases of measuring error disturbing quantities when the recognition error is significant. This also highlights the merit of the proposed method in this paper.

6. Conclusions

This paper proposed a modified extension method with a learning mechanism. When estimating the state-of-health of a lead-acid battery, given the same amount of classical fields, the proposed method can improve lead-acid battery state-of-health estimation accuracy, as compared with the conventional extension theory and extension neural network. Furthermore, for the supervised learning system composed of the proposed modified extension theory and learning mechanism, only the classical fields of various categories of matter-element models are required to optimize output recognition from the training data. With more learning data, future studies can build a more adaptive matter-element model, making the estimation system even more robust.

References

- Unbuku, A. H., & Pascoe, P. E. (2000). VRLA battery state-of-charge estimation in telecommunication power systems. *IEEE Transactions on Industrial Electronics*, 47, 565–573.
- Bose, C. S. C., & Laman, F. C. (2000). Battery state of health estimation through coup de fouet. In *Proceedings of 22nd international telecommunications energy conference* (pp. 597–601).
- Cai, W. (1983). The extension set and incompatibility problem. *Journal of Scientific Exploration*, 1, 81–93.
- Delaille, A., Perrin, M., Huet, F., & Hernout, L. (2006). Study of the coup de fouet of lead-acid cells as a function of their state-of-charge and state-of-health. *Journal of Power Sources*, 158, 1019–1028.
- Jang, J. S. R. (1996). Input Selection for ANFIS Learning. In: *Proceedings of 5th IEEE International Fuzzy System Conference*, 2, 1493–1499.
- Kim, J. H., Lee, S. J., & Cho, B. H. (2009). Discrimination of battery characteristics using discharging/charging voltage pattern recognition. *Proceedings of IEEE Energy Conversion Congress and Exposition*, 1799–1805.

- Lin, C. T., & Lee, C. S. G. (1999). *Neural fuzzy systems: A neuro-fuzzy synergism to intelligent systems*. Englewood Cliffs, New Jersey: Prentice-Hall.
- Oh, S. K., Pedrycz, W., & Park, H. S. (2006). A new approach to the development of genetically optimized multilayer fuzzy polynomial neural networks. *IEEE Transaction on Industrial Electronics*, 53, 1309–1321.
- Pascoe, P. E., & Anbuky, A. H. (2005). Standby power system VRLA battery reserve life estimation scheme. *IEEE Transaction Energy Conversation*, 20, 887–895.
- Pascoe, P. E., & Anbuky, A. H. (2001). Adaptive fuzzy coup de fouet based VRLA battery capacity estimation. *Proceedings of IEEE International System, Man Cybernetics Conference*, 4, 2157–2162.
- Robinson, R. S. (1996). On-line battery testing: A reliable method for determining battery health. In *Proceedings of 18th international telecom. energy conference* (pp. 654–661).
- Shen, W. X., Chan, C. C., Lo, E. W. C., & Chau, K. T. (2002). Adaptive neuro-fuzzy modeling of battery residual capacity for electric vehicles. *IEEE Transaction on Industrial Electronics*, 49, 677–684.
- Spath, V., Jossen, A., Doring, H., & Garche, J. (1997). The detection of the state of health of lead-acid batteries. In: *Proceedings of 19th international telecommunications energy conference* (pp. 681–686).
- Technical Reference Manual for All PSoC Devices with a Base Part Number of CY8C2, XXXX. Available: <http://sjapp20.mis.cypress.com:7001/published-content/publish/design_resources/more_resources/contents/psoc_t>.
- Valdez, M. A. C., Valera, J. A. O., Jojutla, Ma., & Arteaga, O. P. (2006). Estimating SoC in lead-acid batteries using neural networks in a microcontroller-based charge-controller. *Proceedings of International Joint Neural Network Conference*, 2713–2719.
- Wang, M. H. (2003). Extension neural network for power transformer incipient fault diagnosis. *IEE Proceedings Generation, Transmission and Distribution*, 150, 679–685.
- Wang, M. H. (2005). Partial discharge pattern recognition of current transformers using an ENN. *IEEE Transaction Power Delivery*, 20, 1984–1990.
- Wang, M. H., & Ho, C. Y. (2005). Application of extension theory to PD pattern recognition of high voltage current transformers. *IEEE Transactions on Power Delivery*, 20, 1939–1946.
- Wang, C. H., Wang, W. Y., Lee, T. T., & Tseng, P. S. (1995). Fuzzy B-spline membership function (BMF) and its applications in fuzzy-neural control. *IEEE Transactions on Systems, Man and Cybernetics*, 25, 841–851.